New insights into the helicase domain of human Dicer and its biochemical properties: ATPase and RNA rearrangement activities

Kinga Ciechanowska[1], Agnieszka Szczepanska[1] , Kamil Szpotkowski[1] , Klaudia Wojcik[1], Anna Urbanowicz[2] and Anna Kurzynska-Kokorniak[1]*

[1] Department of Ribonucleoprotein Biochemistry, Institute of Bioorganic Chemistry Polish Academy of Sciences, 61-704 Poznan, Poland

[2] Laboratory of Protein Engineering, Institute of Bioorganic Chemistry Polish Academy of Sciences, 61-704 Poznan, Poland

***** Correspondence: akurzyns@man.poznan.pl; Tel.: +48-61-852-8503 (ext. 1264)

Abstract

Dicer ribonucleases are best known for their important role in microRNA and small interfering RNA biogenesis. They may also be involved in chromatin structure remodeling, apoptotic DNA degradation or production of damage-induced small RNAs, which implies that Dicer proteins can interact with many different RNA and DNA substrates. Most Dicers are multi-domain proteins. The here presented studies focus on the human Dicer (hDicer) helicase domain. The hDicer helicase contributes to recognizing pre-miRNA substrates and is suggested to participate in binding of many different cellular RNAs. However, a comprehensive characterization of the biochemical activities and substrate specificity of the hDicer helicase towards different nucleic acids have never been reported. We demonstrate for the first time that the full-length hDicer, through its helicase domain, is capable of ATP hydrolysis. We also show that the hDicer helicase binds only single- but not double-stranded nucleic acids, and that binding of single-stranded RNAs is accompanied by the rearrangement of their structure. The hDicer helicase does not require ATP hydrolysis for this RNA rearrangement activity. Given the documented importance of the hDicer helicase in antiviral defense, the obtained results may contribute to a better understanding of viral diseases and the role of hDicer in virus-host interactions.

1. Introduction

Dicer ribonucleases are the members of the Ribonuclease III (RNase III) family, which are double-stranded RNA (dsRNA) specific endoribonucleases. Human Dicer (hDicer) consists of 1,992 amino acids (~220 kDa) and comprises: an amino (N)-terminal helicase domain, a domain of unknown function (DUF283), Platform, Piwi-Argonaute-Zwille (PAZ) domain, a Connector helix, two RNase III domains (IIIa and IIIb) and a dsRNA-binding domain (dsRBD) (**Figure 1A**) [1]. The Platform-PAZ-Connector helix fragment is often called "the PAZ cassette" [2] or "the PPC cassette" [3]. The three-dimensional structure of hDicer resembles the letter L (**Figure 1B**) [4]. The roles of the individual hDicer domains in binding and processing of its canonical substrates, i.e., single-stranded hairpin precursors of microRNAs (pre-miRNAs), have been studied extensively. The helicase domain selectively interacts with the apical loop of pre-miRNAs, and thus it helps to discriminate among substrates [5, 6]. The DUF283 domain is implicated in the binding of single-stranded nucleic acids [7], and may therefore be also involved in interactions with the apical loop of pre-miRNA hairpins [4]. The PPC cassette anchors the 5' phosphate and 2-nucleotide (nt) 3' overhang of the pre-miRNA substrates [2]. The RNase IIIa and RNase IIIb domains form a single dsRNA-cleavage center [1]. The carboxy (C)-terminal dsRBD has only a supporting role in pre-miRNA binding [8]. dsRBD, together with the helicase and the DUF283 domains, controls the access of a substrate to the catalytic core of hDicer [6, 9].

hDicer is encoded by the *DICER1* gene located on chromosome 14. Originally, the hDicer gene was named "*HERNA*" (HElicase with RNAse motif), because the protein product of the gene contained conservative evolutionary motifs characteristic of the ATP-dependent RNA helicases, i.e., the ATP binding motif and the Asp-Glu-X-Asp/His (DExD/H)-box, and RNA binding motifs [10]. The name "Dicer" was first introduced in 2001, by Bernstein and colleagues [11], and it is derived from the verb "to dice", i.e., the ability of the enzyme to cut dsRNA into uniformly sized ~22-nt RNAs. Because Dicer displayed specificity for dsRNAs, it was assigned to the family of the RNase III endoribonucleases [11].

Of all the Dicer domains, the helicase domain is believed to be one of the most conserved [12]; its sequence is highly similar to the SF2 helicases [13-15]. SF2 is the largest superfamily of helicases and translocases, and enzymes belonging to this superfamily are implicated in diverse cellular processes; e.g., transcription, translation, RNA processing and decay [16]. SF2 is divided into a number of subfamilies including, but not limited to, the DExD/H-box RNA and DNA helicases and RIG-I-like helicases [17]. The DExD/H-box motif (also called the Walker B motif) is essential for ATP hydrolysis and it is present in the helicases which are involved in unwinding dsRNA and double-stranded DNA (dsDNA) structures [16]. The RIG-I motif is found in translocases that move along the dsRNA in an ATP-hydrolysis dependent way [17].

The helicase domain of hDicer consists of three subdomains: HEL1, HEL2i and HEL2, which in the tertiary structure form three lobes (**Figure 1C**) [12]. The HEL1 subdomain contains the DExD/H-box motif, HEL2i includes the RIG-I motif, while the HEL2 subdomain, also called "helicase C", is conserved for all helicases from the DExD/H and the RIG-I-like families of SF2 helicases [18]. It must be emphasized that not all Dicer proteins contain all three helicase subdomains, and some may not contain the helicase domain at all. For example, miRNA-generating Dicer-1 from *Drosophila melanogaster* has a degenerated HEL1 subdomain, which is not capable of ATP hydrolysis [19], the Dicer-type protein from fungus

Magnaporthe oryzae does not have the HEL2i subdomain [20], whereas *Giardia intestinalis* Dicer does not contain the helicase domain [21]. Moreover, the presence of the DExD/H-box and RIG-I motifs does not guarantee that the protein will have the ability to unwind dsRNA or dsDNA, or to translocate. Examples of such proteins include vertebrate Dicers, for which as yet double-stranded nucleic acid unwinding and translocase activities have not been found. In addition, there have been no reports on the ATP-hydrolysis activity of the vertebrate Dicer helicase domains thus far [22]. In contrast, there are several examples of invertebrate, fission yeast or plant Dicer proteins whose helicase domains were reported to display ATP-dependent translocation activity; e.g., *D. melanogaster* Dicer-2 [23], *Caenorhabditis elegans* Dicer [23], *Schizosaccharomyces pombe* Dicer [24] and plant Dicer-like proteins (DCL proteins) from *Arabidopsis thaliana* and *Medicago truncatula* [25-27]. These Dicer-type proteins have also functional RIG-I type subdomains (HEL1, HEL2i and HEL2), which act as a sensor of viral RNAs that activates the appropriate effector RNA interference (RNAi) pathway and, consequently, triggers the degradation of viral RNAs [28]. In vertebrates, a separate protein, the RIG-I helicase, serves as the receptor for the innate immune system during infection by RNA viruses [29]. Once stimulated by the viral dsRNA, the RIG-I receptor initiates the signaling pathways of transcription factors triggering the production of interferon-β and activation of many genes involved in the mobilization of the immune system [30]. It is thought that the helicase domains of vertebrate Dicers have lost their ability to recognize viral dsRNAs because vertebrates developed other intracellular RNA virus sensors; for instance, RIG-I helicases [31]. Consequently, the helicase domains of invertebrate and vertebrate Dicer type-proteins might have developed different functions.

In the organisms that express only one type of Dicer, such as mammals and nematodes, the helicase domain can discriminate between siRNA precursors (pre-siRNAs) and pre-miRNAs [5, 8]; however, the mechanism of this discrimination seems to be different for mammalian and nematode Dicers. The helicase domain of hDicer, by interacting with the apical loop of pre-miRNAs, can distinguish pre-miRNAs from pre-siRNAs [5, 6, 8]. In addition, hDicer processes pre-miRNAs much more efficiently than pre-siRNAs, and the difference in the processing rates between these substrates is attributed to the presence of the helicase domain [8]. It was shown that the deletion of the helicase domain increases the hDicer capability to cleave pre-siRNA substrates [32]. Moreover, the truncated Dicer variant lacking the HEL2i subdomain, found in some mammalian cell lines, was shown to protect tissue stem cells from RNA viruses by dicing viral dsRNA [33]. In the case of nematodes, it was demonstrated that the mutations in the helicase domain of *C. elegans* Dicer, that affect ATP hydrolysis, reduce the amount of certain endogenous siRNAs; however, the same mutations do not affect pre-miRNA and exogenous pre-siRNA processing [34]. It must be noted that most invertebrates separate the processing of pre-miRNA and pre-siRNA substrates between two Dicer proteins: Dicer-1 and Dicer-2, respectively [19, 35]. It was also shown that *C. elegans* Dicer and *D. melanogaster* Dicer-2 cleave pre-siRNA substrates differently, depending on the substrate termini; dsRNAs with blunt termini or 5' overhangs are progressively cleaved in an ATP-dependent manner, whereas substrates with 3' overhangs are distributively cleaved and this process does not require ATP [23]. The cryogenic electron microscopy (cryo-EM) structure of *D. melanogaster* Dicer-2 in complex with a blunt-ended dsRNA revealed that the blunt-ended dsRNA substrates are bound by the helicase domain [36], whereas substrates with 2-nt 3'-overhanging ends are bound by the PPC cassette of Dicer [2].

The helicase domain of Dicer proteins can also serve as a platform for binding of dsRNA Binding Proteins (dsRBPs); e.g., hDicer can form a complex with the TAR RNA-binding protein (TRBP) or the protein activator of protein kinase R (PACT) [37]. TRBP and PACT are important regulators that contribute substrate binding during small regulatory RNA production [38]. In addition, very recently it was shown that hDicer specifically interacts with several dsRBPs and RNA helicases during viral infection [39]. Specifically, proteins such as DExH-Box Helicase 9 (DHX9), adenosine deaminase acting on RNA 1 (ADAR-1) and protein kinase RNA-activated (PKR) are enriched with Dicer in virus-infected cells, and the helicase domain of Dicer was shown to be essential for this interaction [39]. Thus, it is suggested that the helicase domain controls the recruitment of different proteins to diversify the functions of Dicer proteins.

The growing evidence points to possible cleavage-independent regulatory roles of Dicer. For example, it was demonstrated that in *C. elegans* and human cells, Dicer can bind various RNAs, including mRNAs and long noncoding RNAs (lncRNAs), passively, i.e., without further cleavage (so called: “passive binding”) [40]. “Passive sites” present within transcripts were proposed to function as a buffering system to control the cleavage activity of Dicer by sequestering it from pre-miRNAs [40]. Additionally, the interactions between Dicer and mRNA were suggested to regulate the stability of transcripts in the cell [40]. Passive binding of hDicer to cellular transcripts is hypothetically mediated by its helicase domain [40]. Indeed, distribution of the charges on the surface of the helicase domain reveals the positively charged groove, which indicates its potential for nucleic acid binding (**Figure 1D**). Nevertheless, a comprehensive characterization of the biochemical activities of the hDicer’s helicase domain and its substrate specificity towards different nucleic acids have never been reported. The here presented studies provide new insights into the helicase domain of hDicer and its biochemical properties in the context of different RNA and DNA substrates, both single- and double-stranded.

2. Results

2.1. The helicase domain of hDicer is responsible for the ATP hydrolysis activity of hDicer

To investigate biochemical properties of the hDicer helicase domain, we produced this domain as a stand-alone protein, called HEL, in *Escherichia coli* protein expression system (Supplementary **Figure S1**). Because the hDicer helicase domain contains the A Walker motif, which is associated with ATP binding and hydrolysis, in the first step, we tested whether the obtained HEL preparation can bind and hydrolyze ATP. The binding assay was performed by an electrophoretic mobility shift assay (EMSA) and reaction mixtures contained: [γ^{32}P]-ATP substrate (2 nM) and HEL (2 nM). The collected results showed that HEL is able to bind ATP (**Figure 2A**). Next, we analyzed the ATP hydrolysis activity of HEL. As a negative control, in this experiment we applied the hDicer variant lacking the helicase domain (hDicer_ΔHEL); this variant was previously produced and characterized by Y. Lee and colleagues [41]. The [γ^{32}P]-ATP substrate (2 nM) was incubated with HEL (2 nM) or hDicer_ΔHEL (2 nM), and the reaction mixtures were separated by denaturing PAGE and visualized by phosphorimaging. The data collected demonstrated that HEL is able to hydrolyze ATP (**Figure 2B**), such activity was not detected for the hDicer_ΔHEL variant (**Figure 2B**). Consequently, in the next step, we investigated whether the full-length wild-type hDicer (WT hDicer) can perform ATP hydrolysis. The results of the assay involving [γ^{32}P]-

ATP substrate (2 nM) and WT hDicer (2 nM) revealed that hDicer is capable of ATP hydrolysis (**Figure 2C**). The time-course assay involving 2 nM [γ^{32}P]-ATP and HEL (2 nM) or WT hDicer (2 nM) demonstrated that half of the substrate is consumed in ~30 min (**Figure 3**). This result indicated that the helicase domain alone and hDicer display a similar potential to hydrolyze ATP. To the best of our knowledge, the here presented studies show for the first time that hDicer is able to hydrolyze ATP and that the domain responsible for this activity is the helicase domain.

2.2. Nucleic acid binding activity of the hDicer helicase domain

The data collected by A. Rybak-Wolf and colleagues revealed that Dicer enzymes could bind various RNA substrates in the cell, and that binding of some of those substrates was not followed by RNA cleavage [40]. The authors suggested that such passive binding of substrates was mediated by the helicase domain of Dicer [40]. Assuming that the helicase domain of hDicer may play an important role in the binding of various hDicer substrates, we investigated the nucleic acid binding properties of this domain. The binding assays contained the following types of substrates: (i) single-stranded RNAs (ssRNAs), including R10 (12 nt), R20 (21 nt), R30 (32 nt), R40 (42 nt), and R50 (56 nt); (ii) corresponding single-stranded DNAs (ssDNAs), including D10 (12 nt), D20 (21 nt), D30 (32 nt), D40 (42 nt), and D50 (56 nt); (iii) pre-miRNAs, including pre-mir-21, pre-mir-33a, and pre-mir-16-1; (iv) dsRNAs, including dsRNA_blunt (32 base-pair, bp) and dsRNA_over (30 bp with 2-nt 3'-overhangs); and (v) corresponding dsDNAs, including dsDNA_blunt (32 bp) and dsDNA_over (30 bp with 2-nt 3'-overhangs). Single-stranded substrates were ^{32}P-labeled at the 5' ends and double-stranded substrates contained one strand that was 5'-^{32}P-labeled. Before they were applied to the reaction mixtures, ssRNAs and ssDNAs were denatured at 95 °C for 3 min and placed on ice to ensure their single-stranded form. Reaction mixtures containing ~2.5 nM of a substrate and HEL dilutions (2.97, 5.94, 11.86, 23.75, 47.5, 95 μM) were incubated at room temperature for 15 min; then, they were separated using EMSA and visualized by phosphorimaging (**Figure 4**). In general, the observed band patterns indicated that HEL can bind 20-nt ssRNAs and ssDNAs and longer substrates (**Figure 4**). However, in the case of ssRNAs (**Figure 4A**), distinct but low abundant complexes were only observed for R20 and R30 molecules. For R40 and R50 molecules, the RNA•HEL complexes were poorly detected. The ambiguous results and the weak signal made it impossible to determine the K_d values for the ssRNA•HEL complexes. In the case of ssDNAs (**Figure 4B**), we observed distinct ssDNA•HEL complexes for D30, D40 and D50 substrates. The densitometry analyses allowed to calculate K_d values for the D40•HEL and the D50•HEL complexes; these values were: ~8.5 μM for D40•HEL, and ~7.4 μM for D50•HEL.

Taking into consideration the possibility that binding between a nucleic acid and HEL might be unstable during EMSA analysis, we next applied bio-layer interferometry (BLI) to investigate the interactions between ssRNAs or ssDNAs and HEL. BLI is an optic method for studying the affinity between molecules in real time, without needing to use fluorescence or radioisotope-labeled particles. This method is based on using biosensors that are specific to proteins or other substrates which we want to test (e.g., biosensors with Ni-NTA beads are suitable for use with proteins that have His6-tags, as in the case of HEL). BLI can be used to determine the association and dissociation rate constants, as well as the equilibrium dissociation constant (K_d). Given the lack of observed complexes for R10•HEL and D10•HEL (**Figure 4**), in the BLI assay, we used the following ssRNAs: R20, R30, R40, R50.

Additionally, we used the following ssDNAs: D20, D30, D40, D50. The measurements were carried out using HEL (1 μM) and several substrate dilutions (3.125, 6.25, 12.5, 25, 50 and 100 μM). First, HEL was immobilized on Ni-NTA biosensor. After that, HEL-loaded sensor was immersed in a ligand-containing well, to monitor the association, and in a buffer-containing well, to monitor the dissociation of the nucleic acid•protein complex. Each measurement was repeated three times. The collected data revealed that signals were too low to calculate reliable K_d values for the substrates: R20, R30, D20 and D30 (**Figure 5**), although the association and dissociation curves were recorded. The K_d values meeting the quality criteria, calculated based on association and dissociation curves, were collected for: R50•HEL (~23 μM) (**Figure 5A**), D40•HEL (~22 μM) and D50•HEL (~21 μM) (**Figure 5B**). Observed differences in K_d values obtained using EMSA and BLI methods may result from the application of the two different approaches. The BLI method is a more sensitive method, which allows to monitor association and dissociation of complexes in real time. Moreover, in the BLI method we applied the increasing amounts of substrate, while in EMSA we used the increasing amounts of protein. Nevertheless, it is important to note that the K_d values estimated by both methods were at similar micromolar rage.

The next set of binding assays involved pre-miRNA substrates: pre-mir-21, pre-mir-33a, and pre-mir-16-1. The selected pre-miRNAs differ in the compactness of their secondary structures: pre-mir-21 adopts a compact structure, with a small terminal loop, pre-mir-33a contains large internal loops and bulges, but has a small terminal loop, while pre-mir-16-1 has a more relaxed structure, with a 9-nt apical loop (**Figure 6A**). Reaction mixtures containing ~2.5 nM of a substrate and HEL dilutions (11.86, 23.75, 47.5, 95 μM) were incubated at room temperature for 15 min; then, separated using EMSA and visualized by phosphorimaging. The results of the EMSA experiment revealed smeared bands for all reaction sets (**Figure 6B**). Band smearing can be attributed to weak and unstable binding between the pre-miRNA and HEL. The obtained results did not allow to calculate K_d values for the pre-miRNA•HEL complexes.

Finally, the binding assays involving dsRNA and dsDNA substrates were carried out. In the assay, a 32-bp RNA or DNA duplex (blunt) and a 30-bp RNA or DNA duplex with a 2-nt 3' overhang on each end (over), were applied. Thus, in total, we tested four types of substrates: dsRNA_blunt, dsRNA_over, dsDNA_blunt, and dsDNA_over. Double-stranded substrates (~2.5 nM) were incubated with HEL dilutions (2.97, 5.94, 11.86, 23.75, 47.5, 95 μM) at room temperature for 15 min. The results of the EMSA revealed no band-shifts for all tested sets; this indicated that HEL does not bind double-stranded nucleic acids (**Figure 7**).

Altogether, the obtained results revealed that HEL is able to bind single-stranded RNAs and DNAs of 20-nt and longer, and it does not interact with dsRNA and dsDNA substrates. We also found that pre-miRNA substrates, that inherently contain partially double-stranded regions, do not form stable complexes with a stand-alone helicase domain of hDicer.

2.3. The hDicer helicase domain rearranges the structure of interacting RNAs in an ATP-independent way

The results of the EMSA assay revealed weak binding between the ssRNA substrates (R20, R30, R40 and R50) and HEL. Moreover, these results also showed a HEL-concentration-dependent loss of the main substrate form (**Figure 4A**). With this in mind, we hypothesized that HEL might either rearrange the structures of the interacting ssRNA substrates or trigger

their degradation. To test these hypotheses, we investigated the substrates and reaction products of the binding reactions by (i) comparative PAGE, under native and denaturing conditions, and (ii) circular dichroism spectroscopy (CD). All experiments were carried out using the R40 substrate and HEL.

As with the mentioned above binding assays, the reactions that contained ~2.5 nM of ^{32}P-labeled R40 and HEL dilutions (2.97, 5.94, 11.86, 23.75, 47.5, 95 μM) were used. It must be noted that R40, before it was added to the reaction mixtures, was denatured at 95 °C for 3 min; then, it was placed on ice to ensure its single-stranded form. The results of the native PAGE confirmed inefficient formation of complexes between R40 and HEL (**Figure 8A**). We also confirmed the existence of HEL-concentration-dependent loss of the main substrate form (i.e., the R40's slow migrating conformer, presumably represented by a single-stranded form of R40), which was either accompanied by an increase in quantity of the fast migrating conformers of R40 (presumably representing the more compact conformers of R40) or products of R40 degradation. To test the integrity of the substrate after it had interacted with HEL, we separated the reaction mixtures, including R40 and HEL, under denaturing conditions (Supplementary **Figure S2**). Collected results revealed that R40 stayed intact even when the highest concentration of HEL was applied (95 μM). These results proved that R40 does not degrade when incubated with HEL. In the next binding assay we tested the influence of ATP on the observed phenomenon. Moreover, after 15 min incubation of R40 with HEL, with or without 1 mM ATP, SDS was added to the reaction mixtures, to final concentration of 1%. SDS disturbs interactions between proteins and nucleic acids; however, while protein is denatured, the nucleic acid stays structurally intact [37]. The results of the native PAGE showed that, under the applied reaction conditions, with the increase of the HEL concentration, the slower-migrating conformer of R40 gradually disappeared, and the faster-migrating conformers of R40 increased their intensities (**Figure 8B**). The output of the assay did not depend on ATP. Consequently, the collected results indicated that HEL influences R40 structure, and that this process is ATP-independent. We hypothesized that upon HEL binding, R40 can adopt a more compact structure. A possible secondary structure of R40 was predicted by the RNA structure web server [42] (**Figure 8C**). We noticed that the secondary structure of R40 contains double-stranded regions. However, as indicated in **Figure 6,** substrates with double-stranded regions are poorly bound by HEL. To further test the hypothesis that HEL can rearrange the structure of interacting RNAs, we performed the HEL binding assay using a substrate that cannot adopt a secondary structure: a 42-mer composed of $(CU)_{21}$ repeats. This time, with increased HEL concentration, we noticed clear distinct bands correlating to RNA•HEL complexes, and no appearance of the fast migrating conformers (**Figure 8D**). These results further proved that HEL can rearrange the structure of interacting RNAs, providing that RNA has the intrinsic potential to adopt secondary structures. More examples of the HEL-assisted rearrangements of the structure of interacting RNAs can be found in Supplementary **Figure S3.**

In the next set of experiments, we used CD spectroscopy to study the influence of HEL on the R40 structure. CD spectroscopy is a simple optical technique that is most sensitive to the structural polymorphism of nucleic acids and proteins [43]. Due to the fact that the characteristic bands of nucleic acids and proteins in the CD spectrum are separated [44], an independent structural analysis of nucleic acids and proteins can be performed. An analysis of the shape of a CD spectrum provides information on the structure of a biomolecule [45]. CD data are commonly reported as ellipticity (θ), i.e., deviation (flattening) of an ellipse from

the form of a circle or a sphere, usually reported in millidegrees (mdeg). In the experiment, R40 (28 μM) was incubated in a buffer solution (10 mM HEPES pH 8.0, 300 mM NaF) without a protein or with HEL (28 μM); alternatively, HEL (28 μM) was incubated in the buffer solution alone. The samples were incubated at 15 °C. A comparison of the shapes of the CD spectra, in a spectral range of 210 to 350 nm, was generated for the tested samples, and is presented in **Figure 9A**. The tested samples are as follows: (i) HEL, (ii) R40, and (iii) HEL and R40. It must be noted that the helicase domain of hDicer is mostly composed of alpha helices (**Figure 1C**). The ellipticity at 222 nm is routinely used to determine the α-helical content of a protein, and the double-stranded helical regions of RNA give a positive peak at ~270 nm. Our results revealed that the CD spectrum of the HEL protein had a negative minimum value at 222 nm, which is associated with the presence of α-helices. In contrast, the CD spectrum of R40 alone (**Figure 9A**) had a maximum value at ~270 nm, which is characteristic for dsRNA structures [44]. The CD spectrum of the R40•HEL complex had a negative minimum value typical for a protein with a dominant α-helical structure (at 222 nm); however, the maximum value for dsRNA, at ~270 nm, was flattened (**Figure 9A**). This result could be explained by the interactions between HEL and R40, and the structural rearrangements of R40 upon HEL binding.

Next, a thermal analysis of the tested samples was carried out to ascertain the change in ellipticity at 222 nm for the HEL sample (to test the change in α-helical content in the HEL sample) and at 270 nm for the R40 sample (to test the change in dsRNA content in the R40 sample). Regarding the HEL sample (**Figure 9B***),* the value of ellipticity, at 222 nm, increased across the entire range of the tested temperatures (from 5 to 90 °C). Moreover, two discontinuities were visible at ~30 °C and ~60 °C. These discontinuities are called "phase–transition temperatures" [46], and they are associated with the structural changes that occur in a protein due to increases in temperature. More precisely, as the temperature increases, the content of the secondary structure of a protein decreases. For the R40•HEL complex (**Figure 9B**, red dotted curve), the observed discontinuities were shifted towards higher temperatures (i.e., at 52 °C and 74 °C, respectively). This indicates that the structure of HEL stabilized after the R40 binding process occurred.

Next, to investigate the structural changes in R40, thermal analysis was carried out at 270 nm (**Figure 9C**). In the case of R40, as the temperature increased, a decrease in peak intensity was observed. For the R40 sample (**Figure 9C**, black dotted curve), two discontinuities were observed at 35 °C and 75 °C. For the R40•HEL complex (**Figure 9C**, red dotted curve), the discontinuity at ~35 °C was barely visible, and the discontinuity observed at 75 °C, for R40 alone, shifted towards lower temperature, which was 60 °C; thus, the difference in phase transition temperatures, between R40 alone and R40 complexed with HEL, was 15 °C. A comparison of the experimental and theoretical thermodynamic data, with regard to R40 and R40•HEL samples, is attached in Supplementary **Table 1**. Based on the analysis of the thermodynamic parameters, it may be noted that the entropy and enthalpy values for the R40•HEL complex decreased by ~12%, compared with the corresponding values that were generated for R40 alone. These results imply that the structure of R40 was rearranged upon HEL binding.

Together, these data indicate that the helicase domain of hDicer can induce conformational changes in the RNAs with which it interacts.

2.4. RNase activity of the hDicer variant that lacks the helicase domain

The results of the abovementioned experiments indicate that the helicase domain of hDicer interacts with ssRNA substrates (**Figure 4A**), but not with dsRNAs (**Figure 7**). Taking these data into consideration, we then investigated the role of the hDicer helicase domain in the substrate cleavage. We conducted *in vitro* and *in cellulo* experiments, which involved the hDicer_ΔHEL variant [41]. In the *in vitro* RNA cleavage assays, we used two pre-miRNA substrates: pre-mir-21 and pre-mir-16-1. We also used a 30-bp RNA duplex, with a 2-nt 3' overhang on each end (dsRNA_over). The cleavage assays involved 1.25, 2.5, 5, and 10 nM of hDicer_ΔHEL, and ~5 nM of either 5'-^{32}P-labeled pre-mir-21, pre-mir-16-1, or dsRNA_over. The control reactions included 10 nM WT hDicer (hDcr), instead of hDicer_ΔHEL. Two control reactions, without the protein, were also prepared; one contained the substrate in the reaction buffer only (C-), and the other contained the substrate in the reaction buffer with the addition of the Mg^{2+}-chelating agent, EDTA (25 mM). As the Dicer's cleavage activity is dependent on Mg^{2+}, EDTA is able to abrogate this activity. Accordingly, another control reaction included the substrate, protein, and 25 mM EDTA (+EDTA). All reactions were carried out at 37 °C. The reaction mixtures were separated by PAGE under denaturing conditions and visualized by phosphorimaging (**Figure 10**). The results showed that, under the applied reaction conditions, all of the used substrates, namely, pre-mir-21, pre-mir-16-1, and dsRNA_over, were processed more efficiently by the hDicer_ΔHEL variant than by WT hDicer. Densitometric analysis revealed that after 2 hours: ~80% of pre-mir-21 and dsRNA_over, and ~90% of pre-mir-16-1, were cleaved by WT hDicer, and within the same time period, almost all of pre-mir-21, pre-mir-16-1 and dsRNA_over were processed by hDicer_ΔHEL.

Next, we tested the capability of the hDicer_ΔHEL variant to process the endogenous pre-mir-21 and pre-mir-16-1 substrates in living human cells. In the experiments, we used: (i) 293T NoDice cells (the *DICER1* knockout cell line) treated with a transfection reagent only (a negative control); (ii) 293T NoDice cells expressing the hDicer_ΔHEL variant; and (iii) 293T NoDice cells transfected with the plasmid expressing the wild-type full-length hDicer - the WT hDicer (a rescue control). First, the level of produced proteins: hDicer_ΔHEL and WT hDicer was assayed using Western Blot analysis (**Figure 11A**). We found that, 72 h after transfection, the level of hDicer_ΔHEL and WT hDicer was similar (**Figure 11A**). Next, using RT-qPCR, we showed that the relative level of miR-21-5p (**Figure 11B**) and miR-16-1-5p (**Figure 11C**) was lower in the 293T NoDice cells expressing hDicer_ΔHEL than in the 293T NoDice cells expressing WT hDicer. More specifically, miRNA levels were reduced by about ~40% (for both miR-21-5p and miR-16-1-5p), compared with the respective positive control reactions.

Altogether, these data show that the hDicer_ΔHEL variant produces miR-21-5p and miR-16-1-5p more efficiently *in vitro* (**Figure 10**), and it produces miR-21-5p and miR-16-1-5p significantly less efficiently *in cellulo* (**Figure 11**), when compared with WT hDicer. Results of our *in vitro* cleavage assays are in line with the results of the *in vitro* cleavage assays presented by E. Ma and colleagues [47] and D. Zapletal and colleagues [48], who also demonstrated that hDicer variants lacking the helicase domain display higher cleavage potential towards canonical substrates, compared to WT hDicer. Moreover, the results of our RT-qPCR assays showed lower *in cellulo* pre-miRNA processing activity of hDicer_ΔHEL, in comparison to WT hDicer. Importantly, results of these assays are consistent with the results

of RT-qPCR assays carried by E. Kennedy and colleagues [32]. The authors also demonstrated that deletion of the helicase domain from hDicer, reduces its pre-miRNA processing potential *in cellulo* [32].

3. Discussion

In this study, the preparation of the hDicer helicase domain (HEL) obtained in the *E. coli* expression system was applied (Supplementary **Figure S1**). An earlier study, conducted by E. Ma and colleagues demonstrated that the active form of hDicer can be reconstituted from separate domains, including the helicase domain, expressed in *E. coli* [8]. Bacterial expression systems were also successfully used to obtain the active forms of other DExD/H-box helicases [49]. We found that our HEL preparation is able to bind and hydrolyze ATP (**Figure 2A, 2B**), which proves that the hDicer helicase produced in bacteria can be successfully used for biochemical studies.

Importantly, our results of the ATPase activity assays conducted with hDicer (**Figure 2C, 3B**) for the first time demonstrate that the helicase domain of hDicer can hydrolyze ATP. This is in contrast to; e.g., the helicase domain of *D. melanogaster* Dicer-1 that has a degenerated DExD/H-box motif, which exhibits no ATP hydrolysis activity [50]. It must be also mentioned that recently published data by A. Aderounmu and colleagues indicated that ancient Dicers (the ancestors of hDicer) do not display ATPase activity [22]. However, these studies were carried out under high-turnover conditions, with [γ^{32}P]-ATP (100 nM), high excess of non-labeled ATP (100 μM) and the protein preparation of an ancestral Dicer (200 nM). In our assays, we applied approximately the equimolar amounts of substrate and enzyme (2 nM). When we applied similar reaction conditions as A. Aderounmu and colleagues [22], i.e., 1:500 molar ratio of enzyme to substrate, we also did not notice products of ATP hydrolysis in reactions with HEL (Supplementary **Figure S4**). These differences in substrate:enzyme molar ratios may explain the discrepancies in the outputs of the ATP hydrolysis assays carried out by A. Aderounmu and colleagues [22], and by us (**Figure 2C**). It is possible that in the case of substrate excess, the products of ATP hydrolysis, ADP, might inhibit the ATPase activity of the helicase domain. Collectively, results of our studies indicate that hDicer maintains the ATPase activity. Preservation of the ability to hydrolyze ATP by hDicer suggests that this enzyme might exhibit yet unknown activity that is fueled by ATP hydrolysis.

The ends of the pre-miRNA substrate are bound within the PPC cassette of hDicer [2]; however, the single-stranded apical loop region of pre-miRNA interacts with the helicase domain [4]. hDicer may also interact with cellular RNAs other than pre-miRNAs; e.g., with mRNAs or lncRNAs [40]. The binding process for these types of RNA is likely initiated by the helicase domain of hDicer [40]. These observations prompted us to investigate the substrate specificity of the hDicer helicase domain. The *in vitro* binding assays revealed that the helicase domain was capable of binding ~20-nt ssRNAs, ssDNAs, and longer substrates (**Figure 4**); however, binding of pre-miRNAs, which have partially double-stranded structures, was very inefficient (**Figure 6**). The dsRNA and dsDNA substrates were not bound by the hDicer helicase (**Figure 7**). The most likely explanation for these observations are the structural constraints of the hDicer helicase domain [4]. A comparison of the tertiary structures of *A. thaliana* DCL1 [51], *D. melanogaster* Dicer-2 [52], and hDicer [4] indicates that both *A. thaliana* DCL1 and *D. melanogaster* Dicer-2 have a wide cleft within their helicase domains, that can embrace double-stranded regions of primary pre-miRNA

precursors (pri-miRNA) and pre-miRNA substrates. Conversely, the hDicer helicase domain has a much narrower cleft that cannot accommodate dsRNAs [4].

In the EMSA analysis, for ssRNA substrates we noticed the HEL-concentration-dependent loss of the main substrate form (**Figure 4A, Figure 8A,** Supplementary **Figure S3**). The most plausible reason for the observed phenomenon is the rearrangement of the structure of RNAs by the hDicer helicase, as demonstrated by comparative PAGE under native and denaturing conditions (**Figure 8B**, Supplementary **Figure S2**) and CD spectroscopy (**Figure 9**) studies. Our observations are in line with the results of the structural studies carried out for *Mus musculus* Dicer in the complex with pre-miRNA [48]. Taking into consideration these data, we can assume that upon binding of pre-miRNA, Dicer, through its helicase domain, induces structural changes within the apical loop of pre-miRNA. These structural rearrangements may result in a better fitting of the substrate into the catalytic site, and consequently, a more precise substrate cleavage [48]. Indeed, in cells producing hDicer variant lacking the helicase domain, non-homogeneous miRNA pool was observed [48]. The structural studies of the mouse pre-miRNA•Dicer complex revealed also the two-step mechanism of pre-miRNA cleavage by Dicer, as follows: (i) Dicer locked in the closed state recognizes pre-miRNA and forms the pre-cleavage state and (ii) Dicer switches into the open state that allows loading of pre-miRNA into the catalytic site of Dicer [48]. The Dicer's helicase domain plays a unique structural role in this process, i.e., it locks Dicer in the closed state, which facilitates pre-miRNA selection. Transition to the cleavage-competent open state is stimulated by Dicer-binding partner TRBP [48]. Such a scenario of miRNA biogenesis is also very likely for hDicer, as it was presented recently by Y. Lee and colleagues [6]. These structural data can also explain the observed differences in pre-miRNA processing under *in vitro* (**Figure 10**) and *in cellulo* (**Figure 11**) conditions. As demonstrated by our *in vitro* cleavage assays (**Figure 10**) and earlier *in vitro* studies conducted by E. Ma and colleagues [47] and D. Zapletal and colleagues [48], the lack of the helicase domain increases the hDicer cleavage efficiency. Presumably, under *in vitro* conditions, the presence of the helicase domain slows down the Dicer's ability to process pre-miRNA because of the time taken to bind and rearrange a single-stranded apical region of a pre-miRNA substrate. However, in the cell, the pre-miRNA processing conditions are quite different. Dicer that lacks the helicase domain cannot interact with its protein partners, such as TRBP; consequently, it is not capable of efficiently adopting the cleavage-competent open state that is necessary for effective pre-miRNA processing. This hypothesis is supported by our data (**Figure 11**) and also the data collected by E. Kennedy and colleagues who showed that the hDicer_ΔHEL variant produces fewer miRNAs under *in cellulo* conditions than full-length hDicer [32]. Structural data collected for *D. melanogaster* Dicer-2 [52] and *A. thaliana* DCL1 [51] also indicate that the proper orientation of the helicase domain is crucial for the specific recognition and binding of a substrate, as well as its further processing. We may further speculate that the helicase domain orchestrates the binding of a substrate that is not followed by Dicer cleavage; the passive binding of cellular RNAs has already been reported by A. Rybak-Wolf and colleagues [40].

Due to the steric constraints, the RIG-I subdomains of the vertebrate Dicers presumably are not capable of recognizing viral dsRNAs to activate antiviral immunity [31]; this contrasts with the RIG-I subdomains that are present in insect [28, 53] and plant [54, 55] Dicer proteins. However, recent literature data indicate the important role of the hDicer helicase domain in triggering antiviral responses [39]. Results of this study show that the hDicer

helicase, during viral infections, binds to proteins which are involved in the antiviral response, such as DHX9, ADAR-1, and PKR kinase [39]. We truly believe that the results of our study will help to better understand the role of hDicer in the cellular processes extending beyond the small RNA biogenesis pathways.

4. Materials and Methods

4.1. Oligonucleotides

DNA and RNA oligonucleotides were purchased from Genomed (Warsaw, Poland) and FutureSynthesis (Poznan, Poland), respectively. Sequences of all oligonucleotides used in this study are listed in Table 1.

Table 1. Sequences of the oligonucleotides used in the experiments.

Name	Sequence (5' → 3')
pre-mir-21	AGCUUAUCAGACUGAUGUUGACUGUUGAAUCUCAUGGCAACACCAGUCGAUGGGCUGU
pre-mir-16-1	UAGCAGCACGUAAAUAUUGGCGUUAAGAUUCUAAAAUUAUCUCCAGUAUUAACUGUGCUGCUGAA
pre-mir-33a	GUGCAUUGUAGUUGCAUUGCAUGUUCUGGUGGUACCCAUGCAAUGUUUCCACAGUGCAUC
R30*	GUGCAUUGUAGUUGCAUUGCAUGUUCUGGUCA
R30_over	ACCAGAACAUGCAAUGCAACUACAAUGCACAU
R30_blunt	UGACCAGAACAUGCAAUGCAACUACAAUGCAC
R12	GAAUCUUAACGC
R21	UCGAAGUAUUCCGCGUACGUG
R42	GGGAGAAUCAUAAGUAGCCUCCCCCCAUGUUAACAGUUAGCC
R56	GGGAGAAUCAUAAGUAGCGCAGUGAGUCGUUGUGCUGCCCAUGUUAACAGUUAGCC
D30**	GTGCATTGTAGTTGCATTGCATGTTCTGGTCA
D30_over	ACCAGAACATGCAATGCAACTACAATGCACAT
D30_blunt	TGACCAGAACATGCAATGCAACTACAATGCAC
D12	GAATCTTAACGC
D21	TCGAAGTATTCCGCGTACGTG
D42	GGGAGAATCATAAGTAGCCTCCCCCCATGTTAACAGTTAGCC
D56	GGGAGAATCATAAGTAGCGCAGTGAGTCGTTGTGCTGCCCATGTTAACAGTTAGCC
f.miR-21-5p	GCTTATCAGACTGATGTTGAAA
f.miR-16-1-5p	GCACGTAAATATTGGCGAA
$(CU)_{21}$	CUCUCUCUCUCUCUCUCUCUCUCUCUCUCUCUCUCUCUCUCU

*R30 serves as a complementary strand to R30_over and R30_blunt to form dsRNAs with a 2-nt 3' overhang or a blunt end, respectively.

** D30 serves as a complementary strand to D30_over and D30_blunt to form dsDNAs with a 2-nt 3' overhang or a blunt end, respectively.

4.2.^{32}P labeling of oligonucleotides

The 5'-end labeling of oligonucleotides was performed according to the previously described procedure [56].

4.3. Preparation of dsRNA and dsDNA

To prepare dsRNA and dsDNA substrates, non-labeled strand (R30_sense/D30_sense or R30_over/D30_over) was hybridized, at a molar ratio of approximately 1:1, with ^{32}P-labeled complementary strand (R30/D30) in buffer containing 50 mM NaCl, 2.5 mM $MgCl_2$ and 20 mM Tris-HCl, pH 7.5, by heating up to 95 °C and then slowly cooling down to room temperature. Next, the reaction mixtures were PAGE-purified with 12% native PAA gels to obtain pure, double-stranded fractions free of single-stranded species.

4.4. ATP hydrolysis and binding assays

The reactions were carried out in 10-µl volumes. HEL (2 nM) or WT hDicer (2 nM) and hDicer_ΔHEL (2 nM) was added to 10,000 cpm (2 nM) [γ^{32}P]-ATP (Hartman Analytic, Braunschweig, Germany) and incubated in binding buffer (50 mM NaCl, 150 mM Tris-HCl pH 7.5) with 2.5 mM $MgCl_2$ for 30 min at 37 °C. Control reactions were prepared without protein. The reactions were separated in 10% native PAA gels at 4 °C in 1x TBE running buffer (for binding assay) or in 15% denaturing PAA gels in 1x TBE running buffer (for hydrolysis assay). The data were collected using a Amersham™ Typhoon™ (Cytiva, Washington, D.C., USA) and quantified using MultiGauge 3.0 (Fujifilm, Tokyo, Japan). The ATP hydrolysis and binding assays were conducted in triplicate.

4.5. Binding assay

The reactions were carried out in 40-µl volumes. HEL (2.97, 5.94, 11.86, 23.75, 47.5, 95 µM) was added to 10,000 cpm (2.5 nM) of ^{32}P-labeled RNA, DNA, dsRNA or double-stranded DNA (dsDNA) and incubated in binding buffer (50 mM NaCl, 150 mM Tris-HCl pH 7.5) for 15 min at room temperature. Control reactions were prepared without protein. The reactions were separated in 5% native PAA gels at 4 °C in 1x TBE running buffer. The data were collected using a Amersham™ Typhoon™ (Cytiva, Washington, D.C, USA) and quantified using MultiGauge 3.0 (Fujifilm, Tokyo, Japan). Binding assays were conducted in triplicate.

4.6. Data analysis

Binding assay results were used to estimate the equilibrium dissociation constant (K_d). K_d was estimated on the basis of densitometry analysis in Multi Gauge software (Fujifilm, Tokyo, Japan). K_d was calculated using formula:

$f = A*P_0/(P_0 + K_d)$,

where: f - fraction of bound substrate; P_0 - molar concentrations of the protein (µM); A - maximum RNA/DNA bound (%). K_d was calculated for f = 0.5 (half of the substrate is bound). P_0 was a protein concentration, for which 50% of substrate was bound. K_d values were calculated based on results from three experiments.

4.7. Bio-Layer Interferometry (BLI)

The measurements were carried out in 200-µl volumes on black 96-well plates (Greiner bio-one, Kremsmünster, Austria) using Octet K2 (ForteBio, Pall Life Sciences, New York, USA) and Octet NTA biosensors (Sartorius, Göttingen, Germany). HEL (1 µM) was incubated with ssRNAs: R20, R30, R40, R50; or ssDNAs: D20, D30, D40, D50 in binding buffer (50 mM NaCl, 150 mM Tris-HCl pH 7.5); increasing amounts of substrate were used: 3.125 µM, 6.25 µM, 12.5 µM, 25 µM, 50 µM, 100 µM. After each measurement, HEL buffer (50 mM HEPES buffer pH 7.5, 0.5 M NaCl, 0.1% Triton X-100 and 5% glycerol), glycine (10 mM, pH 1.7) and $NiSO_4$ (10 mM) were used for neutralization and regeneration of Ni-NTA sensor. Measurements were carried out at 23 °C with shaking speed 1,000 rpm and according to following steps: Loading (1 800 s), Baseline (60 s), Association (20 s), Dissociation (20 s), Neutralization (3x 30 s), Regeneration (60 s). Each measurement included a parallel reference, in which HEL-loaded biosensors were immersed in the binding buffer only instead of the serial dilutions of the ligand. Reference subtracted BLI response curves were generated and used for the determination of the K_d constant and its error. Inter-step correction and Y-alignment were used to minimize tip-dependent variability. Data were collected and globally fitted by a 1:1 stoichiometry model using the Data Acquisition and Data Analysis Software vHT 11.1 (ForteBio, Pall Life Sciences, New York, USA). The fitting met the quality criteria $\chi 2 < 3$ and $R2 \geq 0.96$.

4.8. Circular Dichroism (CD)

Circular dichroism spectra were collected on J-815 CD spectrometer (JASCO, Tokyo, Japan) equipped with a Peltier thermostatic cell holder. HEL (28 µM), RNA (28 µM), and RNA•HEL complexes (molar ratio 1:1) were placed in the buffer containing: 10 mM HEPES pH 8.0, 300 mM NaF, analyzed in a 0.1 cm quartz cuvette (Hellma 100-QS, Jena, Germany). Each CD spectrum was generated based on 9 scans in continuous scanning mode, with a scanning speed of 50 nm min^{-1}, a 1 nm bandwidth, a 0.5 nm data pitch and a data integration time 1 s. When collecting a regular spectrum, data were gathered at wavelengths ranging from 210 to 350 nm for the thermal melt analysis. Thermal analysis were done in the range from 5 to 90 °C. Buffer subtraction and all spectra processing were made using the Jasco Spectra Menager software and Savitzky-Golay tool with a smoothing window of 10 points. The normalized root mean square deviation (NRMSD) for each CD spectrum analysis was less than 0.1. CD data are presented in terms of ellipticity values, in millidegrees (mdeg).

4.9. Cell culture and transfection

293T NoDice cells [57] were cultured in DMEM (Gibco, Thermo Fisher Scientific, Waltham, MA, USA) supplemented with 10% FBS (Gibco, Thermo Fisher Scientific, Waltham, MA, USA), Penicillin-Streptomycin (100 U/mL of penicillin and 100 µg/mL of streptomycin, Gibco) and 1 mM Sodium Pyruvate (Gibco, Thermo Fisher Scientific, Waltham, MA, USA), as described in Bogerd and colleagues [57]. Transfections were performed using the wild-type hDicer and hDicer_ΔHEL expression plasmids, was carried out by DharmaFECT kb DNA Transfection Reagent (Dharmacon, Lafayette, CO, USA) according to the manufacturer's instructions. 293T NoDice cell line was kindly provided by Prof. Bryan R. Cullen [57].

4.10. Protein preparations used in the studies

The HEL cDNA (1-624 aa hDicer) was amplified by PCR using a purchased plasmid encoding a complete *Homo sapiens* Dicer1 ribonuclease type III sequence (PubMed, NM_030621) (GeneCopoeia, Rockville, MD, USA). Obtained fragment was cloned into pMCSG7 vector (courtesy of Laboratory of Protein Engineering, Institute of Bioorganic Chemistry, Polish Academy of Sciences), which introduces a His6-tag at the N-terminus of the protein. HEL was expressed in *E. coli* strain BL21Star (Thermo Fisher Scientific, Waltham, MA, USA) in standard Luria-Bertani (LB) medium. *E. coli* cells were treated with 0.4 mM IPTG and cultured 18 hours at 18 °C with shaking. The cell pellets were lysed and purified using Ni^{2+}-Sepharose High Performance beads (Cytiva, Washington, D.C., USA) with and imidazole gradient (0.02 M – 1 M) in 0.05 mM HEPES buffer (pH 7.5) supplemented with 0.5 M NaCl, 0.1% Triton X-100 and 5% glycerol. The proteins purity were assessed by SDS-PAGE. Protein was concentrated using Amicon filters (Merck, Darmstadt, Germany) in the buffer (50 mM HEPES pH 7.5, 500 mM NaCl, 0.1% Triton X-100, 5% glycerol) and stored at 4 °C.

The expression plasmid encoding the wild-type hDicer was prepared as described previously [58]. In brief, the expression plasmid was obtained by using PCR amplification. All primers were designed based on the cDNA encoding transcript 2 of human *DICER1* (NM_030621.4). The obtained PCR product was applied to prepare expression plasmid using SureVector system (Agilent, Santa Clara, CA, USA), according to the manufacturer's instructions. The expression plasmid encoding the hDicer_ΔHEL variant was purchased from Addgene (#51366) [41].

The wild-type hDicer and hDicer_ΔHEL were produced and purified according to the previously described procedure [58]. Obtained hDicer and hDicer_ΔHEL proteins were examined using Western blot analysis according to the previously described procedure [58].

4.11. The RNA cleavage assay

The RNA cleavage assays were performed according to the previously described procedure [58].

4.12. Reverse transcription and quantitative PCR

RNA was extracted using a standard TRIzol protocol (Invitrogen, Waltham, MA, USA). The quantity and quality of the RNA were measured using the NanoDrop 2000 (Thermo Fisher Scientific, Waltham, MA, USA). For reverse transcription (RT), 8 µg of the total RNA was used. RT was performed with the Mir-X™ miRNA First-Strand Synthesis Kit (Takara Bio, Canada, USA), which was used in accordance with the manufacturer's instructions. RT-qPCR was performed according to the the previously described procedure [56]. The primer sequences used for qRT-PCR are listed in Table 1.

4.13. Gel imaging and analysis

The data were collected using a Amersham™ Typhoon™ (Cytiva, Washington, D.C., USA) and quantified using MultiGauge 3.0 software (Fujifilm, Minato, Tokyo, Japan). Data from qPCR analysis were created using Prism 8.2.1 (GraphPad, San Diego, CA, USA). In the

case of all diagrams, error bars represent SD values calculated based on three independent experiments.

Supplementary Materials: Figure S1: SDS-PAGE gel showing the hDicer helicase domain preparation (HEL) used in the studies. **Figure S2**: Denaturing PAGE analysis of 5′-^{32}P-R40 (2.5 nM) incubated with increasing amounts of HEL. **Figure S3**: Interactions between ssRNAs (R30, R50) and HEL. **Figure S4**: Time dependent ATP hydrolysis by HEL under high-turnover and low-turnover conditions. **Table S1**: Comparison of the theoretical and experimental thermodynamic parameters for R40 and the R40•HEL complex.

Author Contributions: K.C., A.S., K.S., K.W. and A.U. planned and performed experiments: K.C. produced the HEL protein preparation, conducted binding assays, and BLI experiments; A.S. produced hDicer_ΔHEL protein preparation, conducted the RNase assays, Western blots and RT-qPCR assays; K.S. conducted CD measurements; K.W. produced WT hDicer protein preparation; A.U. conducted BLI measurements; all authors analyzed the data and interpreted the results; A.K.K. conceived the studies, coordinated the research, supervised and provided advice; K.C. and A.S. wrote the draft of the manuscript; A.K.K. revised and edited the manuscript and was responsible for its final form. All authors have read and agreed to the published version of the manuscript.

Funding: This work was supported by the National Science Centre, Poland (NCN, grant SONATA BIS 2016/22/E/NZ1/00422 to A.K.K. and NCN, grant PRELUDIUM 2021/41/N/NZ2/03849 to K. C.).

Data Availability Statement: Not applicable.

Acknowledgments: We would like to thank Prof. Bryan R. Cullen for generously providing Dicer-deficient (NoDice) 293T human cell lines and Marta Wojnicka for providing the construct encoding WT hDicer.

Conflicts of Interest: The authors declare no conflict of interest.

References

1. Zhang, H., et al., *Single processing center models for human Dicer and bacterial RNase III.* Cell, 2004. **118**(1): p. 57-68.
2. Tian, Y., et al., *A Phosphate-Binding Pocket within the Platform-PAZ-Connector Helix Cassette of Human Dicer.* Mol Cell, 2014. **53**(4): p. 606-16.
3. Koralewska, N., et al., *Human ribonuclease Dicer – structure and functions.* Postepy Biochem, 2019. **65**(3): p. 173-182.
4. Liu, Z., et al., *Cryo-EM Structure of Human Dicer and Its Complexes with a Pre-miRNA Substrate.* Cell, 2018. **173**(6): p. 1549-1550.
5. Taylor, D.W., et al., *Substrate-specific structural rearrangements of human Dicer.* Nat Struct Mol Biol, 2013. **20**(6): p. 662-70.
6. Lee, Y.Y., et al., *Structure of the human DICER-pre-miRNA complex in a dicing state.* Nature, 2023. **615**(7951): p. 331-338.
7. Kurzynska-Kokorniak, A., et al., *Revealing a new activity of the human Dicer DUF283 domain in vitro.* Sci Rep, 2016. **6**: p. 23989.
8. Ma, E., et al., *Coordinated activities of human dicer domains in regulatory RNA processing.* J Mol Biol, 2012. **422**(4): p. 466-76.

9. Wostenberg, C., et al., *The role of human Dicer-dsRBD in processing small regulatory RNAs.* PLoS One, 2012. **7**(12): p. e51829.
10. Matsuda, S., et al., *Molecular cloning and characterization of a novel human gene (HERNA) which encodes a putative RNA-helicase.* Biochim Biophys Acta, 2000. **1490**(1-2): p. 163-9.
11. Bernstein, E., et al., *Role for a bidentate ribonuclease in the initiation step of RNA interference.* Nature, 2001. **409**(6818): p. 363-6.
12. Kidwell, M.A., J.M. Chan, and J.A. Doudna, *Evolutionarily conserved roles of the dicer helicase domain in regulating RNA interference processing.* J Biol Chem, 2014. **289**(41): p. 28352-62.
13. Aravind, L., D.R. Walker, and E.V. Koonin, *Conserved domains in DNA repair proteins and evolution of repair systems.* Nucleic Acids Res, 1999. **27**(5): p. 1223-42.
14. Lestini, R., F. Delpech, and H. Myllykallio, *DNA replication restart and cellular dynamics of Hef helicase/nuclease protein in Haloferax volcanii.* Biochimie, 2015. **118**: p. 254-63.
15. Shabalina, S.A. and E.V. Koonin, *Origins and evolution of eukaryotic RNA interference.* Trends Ecol Evol, 2008. **23**(10): p. 578-87.
16. Singleton, M.R., M.S. Dillingham, and D.B. Wigley, *Structure and mechanism of helicases and nucleic acid translocases.* Annu Rev Biochem, 2007. **76**: p. 23-50.
17. Byrd, A.K. and K.D. Raney, *Superfamily 2 helicases.* Front Biosci (Landmark Ed), 2012. **17**: p. 2070-88.
18. Zou, J., et al., *Origin and evolution of the RIG-I like RNA helicase gene family.* BMC Evol Biol, 2009. **9**: p. 85.
19. Lee, Y.S., et al., *Distinct roles for Drosophila Dicer-1 and Dicer-2 in the siRNA/miRNA silencing pathways.* Cell, 2004. **117**(1): p. 69-81.
20. Kadotani, N., et al., *One of the two Dicer-like proteins in the filamentous fungi Magnaporthe oryzae genome is responsible for hairpin RNA-triggered RNA silencing and related small interfering RNA accumulation.* J Biol Chem, 2004. **279**(43): p. 44467-74.
21. Macrae, I.J., et al., *Structural basis for double-stranded RNA processing by Dicer.* Science, 2006. **311**(5758): p. 195-8.
22. Aderounmu, A.M., et al., *Ancestral protein reconstruction reveals evolutionary events governing variation in Dicer helicase function.* Elife, 2023. **12**.
23. Welker, N.C., et al., *Dicer's helicase domain discriminates dsRNA termini to promote an altered reaction mode.* Mol Cell, 2011. **41**(5): p. 589-99.
24. Colmenares, S.U., et al., *Coupling of double-stranded RNA synthesis and siRNA generation in fission yeast RNAi.* Mol Cell, 2007. **27**(3): p. 449-61.
25. Tworak, A., et al., *Six Medicago truncatula Dicer-like protein genes are expressed in plant cells and upregulated in nodules.* Plant Cell Rep, 2016. **35**(5): p. 1043-52.
26. Liu, C., M.J. Axtell, and N.V. Fedoroff, *The helicase and RNaseIIIa domains of Arabidopsis Dicer-Like1 modulate catalytic parameters during microRNA biogenesis.* Plant Physiol, 2012. **159**(2): p. 748-58.
27. Fukudome, A. and T. Fukuhara, *Plant dicer-like proteins: double-stranded RNA-cleaving enzymes for small RNA biogenesis.* J Plant Res, 2017. **130**(1): p. 33-44.
28. van Rij, R.P., et al., *The RNA silencing endonuclease Argonaute 2 mediates specific antiviral immunity in Drosophila melanogaster.* Genes Dev, 2006. **20**(21): p. 2985-95.
29. Ahmad, S. and S. Hur, *Helicases in Antiviral Immunity: Dual Properties as Sensors and Effectors.* Trends Biochem Sci, 2015. **40**(10): p. 576-585.
30. Kowalinski, E., et al., *Structural basis for the activation of innate immune pattern-recognition receptor RIG-I by viral RNA.* Cell, 2011. **147**(2): p. 423-35.
31. Hansen, S.R., et al., *Dicer's Helicase Domain: A Meeting Place for Regulatory Proteins.* Cold Spring Harb Symp Quant Biol, 2019. **84**: p. 185-193.
32. Kennedy, E.M., et al., *Production of functional small interfering RNAs by an amino-terminal deletion mutant of human Dicer.* Proc Natl Acad Sci U S A, 2015. **112**(50): p. E6945-54.

33. Poirier, E.Z., et al., *An isoform of Dicer protects mammalian stem cells against multiple RNA viruses.* Science, 2021. **373**(6551): p. 231-236.
34. Welker, N.C., et al., *Dicer's helicase domain is required for accumulation of some, but not all, C. elegans endogenous siRNAs.* RNA, 2010. **16**(5): p. 893-903.
35. Mukherjee, K., H. Campos, and B. Kolaczkowski, *Evolution of animal and plant dicers: early parallel duplications and recurrent adaptation of antiviral RNA binding in plants.* Mol Biol Evol, 2013. **30**(3): p. 627-41.
36. Sinha, N.K., et al., *Dicer uses distinct modules for recognizing dsRNA termini.* Science, 2018. **359**(6373): p. 329-334.
37. Kedersha, N.L. and L.H. Rome, *Isolation and characterization of a novel ribonucleoprotein particle: large structures contain a single species of small RNA.* J Cell Biol, 1986. **103**(3): p. 699-709.
38. Lee, H.Y., et al., *Differential roles of human Dicer-binding proteins TRBP and PACT in small RNA processing.* Nucleic Acids Res, 2013. **41**(13): p. 6568-76.
39. Montavon, T.C., et al., *Human DICER helicase domain recruits PKR and modulates its antiviral activity.* PLoS Pathog, 2021. **17**(5): p. e1009549.
40. Rybak-Wolf, A., et al., *A variety of dicer substrates in human and C. elegans.* Cell, 2014. **159**(5): p. 1153-1167.
41. Lee, Y., et al., *The role of PACT in the RNA silencing pathway.* EMBO J, 2006. **25**(3): p. 522-32.
42. Mathews, D.H., D.H. Turner, and R.M. Watson, *RNA Secondary Structure Prediction.* Curr Protoc Nucleic Acid Chem, 2016. **67**: p. 11.2.1-11.2.19.
43. Kelly, S.M. and N.C. Price, *The use of circular dichroism in the investigation of protein structure and function.* Curr Protein Pept Sci, 2000. **1**(4): p. 349-84.
44. Ma, Y., K. Iida, and K. Nagasawa, *Topologies of G-quadruplex: Biological functions and regulation by ligands.* Biochem Biophys Res Commun, 2020. **531**(1): p. 3-17.
45. B.A., W., et al., *Synchrotron radiation circular dichroism (SRCD) spectroscopy: An emerging method in structural biology for examining protein conformations and protein interactions,*. 2011, Nuclear Instruments and Methods in Physics Research Section A: Accelerators, Spectrometers, Detectors and Associated Equipment. p. 177-178.
46. Vekilov, P.G., *Phase diagrams and kinetics of phase transitions in protein solutions.* J Phys Condens Matter, 2012. **24**(19): p. 193101.
47. Ma, E., et al., *Autoinhibition of human dicer by its internal helicase domain.* J Mol Biol, 2008. **380**(1): p. 237-43.
48. Zapletal, D., et al., *Structural and functional basis of mammalian microRNA biogenesis by Dicer.* Mol Cell, 2022. **82**(21): p. 4064-4079.e13.
49. Muller, U.F. and H.U. Goringer, *Mechanism of the gBP21-mediated RNA/RNA annealing reaction: matchmaking and charge reduction.* Nucleic Acids Res, 2002. **30**(2): p. 447-55.
50. Jiang, F., et al., *Dicer-1 and R3D1-L catalyze microRNA maturation in Drosophila.* Genes Dev, 2005. **19**(14): p. 1674-9.
51. Wei, X., et al., *Structural basis of microRNA processing by Dicer-like 1.* Nat Plants, 2021. **7**(10): p. 1389-1396.
52. Su, S., et al., *Structural insights into dsRNA processing by Drosophila Dicer-2-Loqs-PD.* Nature, 2022. **607**(7918): p. 399-406.
53. Kemp, C. and J.L. Imler, *Antiviral immunity in drosophila.* Curr Opin Immunol, 2009. **21**(1): p. 3-9.
54. Voinnet, O., *Induction and suppression of RNA silencing: insights from viral infections.* Nat Rev Genet, 2005. **6**(3): p. 206-20.
55. Baulcombe, D., *RNA silencing in plants.* Nature, 2004. **431**(7006): p. 356-63.
56. Szczepanska, A., M. Wojnicka, and A. Kurzynska-Kokorniak, *The Significance of the DUF283 Domain for the Activity of Human Ribonuclease Dicer.* Int J Mol Sci, 2021. **22**(16).

57. Bogerd, H.P., et al., *Derivation and characterization of Dicer- and microRNA-deficient human cells.* RNA, 2014. **20**(6): p. 923-37.
58. Wojnicka, M., A. Szczepanska, and A. Kurzynska-Kokorniak, *Unknown Areas of Activity of Human Ribonuclease Dicer: A Putative Deoxyribonuclease Activity.* Molecules, 2020. **25**(6).

Figures

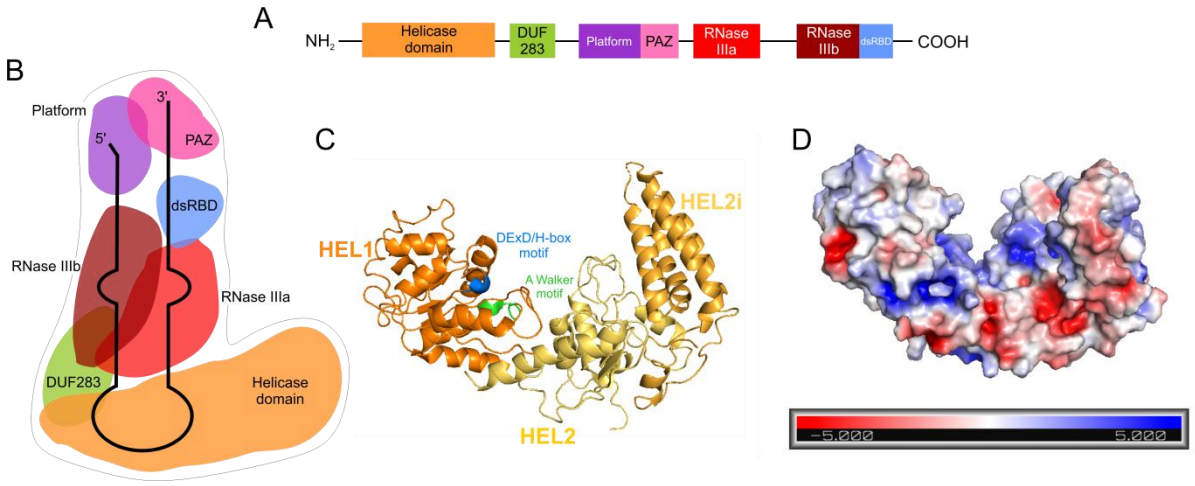

Figure 1. Architecture of human ribonuclease Dicer (hDicer) and its helicase domain. (A) Scheme showing the domain organization in the primary structure of hDicer, based on Liu and colleagues, 2012 [26]. **(B)** Scheme of the tertiary structure of hDicer with a miRNA precursor (pre-miRNA), based on Taylor and colleagues, 2013 [5] and Liu and colleagues, 2018 [4]. **(C)** The tertiary structure of the hDicer helicase domain (PDB 5ZAL) visualized using PyMOL. Three subdomains: HEL1, HEL2i and HEL2 are distinguished, and DExD/H-box and A Walker motifs are indicated. **(D)** The distribution of charges on the surface of the helicase domain (PDB 5ZAL) visualized using PyMOL.

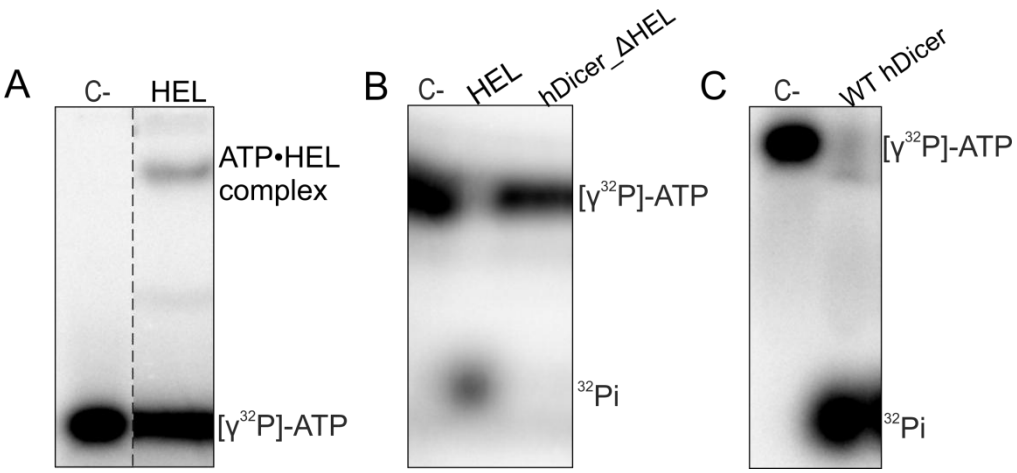

Figure 2. ATP binding and ATP hydrolysis by the hDicer helicase domain (HEL), the hDicer variant lacking the helicase domain (hDicer_ΔHEL) and wild-type hDicer (WT hDicer). (A) Electrophoretic mobility shift assay (EMSA) with HEL (2 nM) and [γ^{32}P]-ATP (2 nM). **(B, C)** Denaturing polyacrylamide gel electrophoresis (PAGE) analysis of the mixtures of [γ^{32}P]-ATP (2 nM) and **(B)** the HEL (2 nM) and the hDicer_ΔHEL variant (2 nM), **(C)** WT hDicer (2 nM). Reaction mixtures were incubated at 37 °C for 30 min. (C-) − a control sample with no protein. (^{32}Pi) - a product of [γ^{32}P]-ATP hydrolysis.

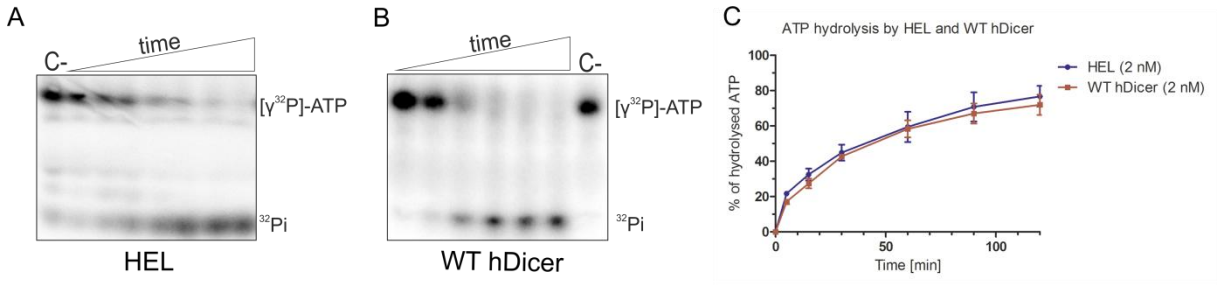

Figure 3. Time-dependent ATP hydrolysis activity of HEL and WT hDicer. (A) Denaturing PAGE analysis of the mixtures of [γ^{32}P]-ATP (2 nM) and HEL (2 nM). The triangle represents time at: 0, 5, 15, 30, 60, 90 and 120 min, reaction mixtures were incubated at 37 °C, (C-) − a control sample with no protein, (^{32}Pi) - a product of [γ^{32}P]-ATP hydrolysis. **(B)** Denaturing PAGE analysis of the mixtures of [γ^{32}P]-ATP and WT hDicer (2 nM). The triangle represents time at: 0, 5, 30, 60, 90 and 120 min, reaction mixtures were incubated at 37 °C, (C-) − a control sample with no protein, (^{32}Pi) - a product of [γ^{32}P]-ATP hydrolysis. **(C)** Graphic presentation of the obtained results. The *x*-axis represents the incubation time expressed in minutes, and the *y*-axis represents the percentage of hydrolyzed ATP by HEL and WT hDicer. Error bars represents standard deviations (SD) from three separate experiments.

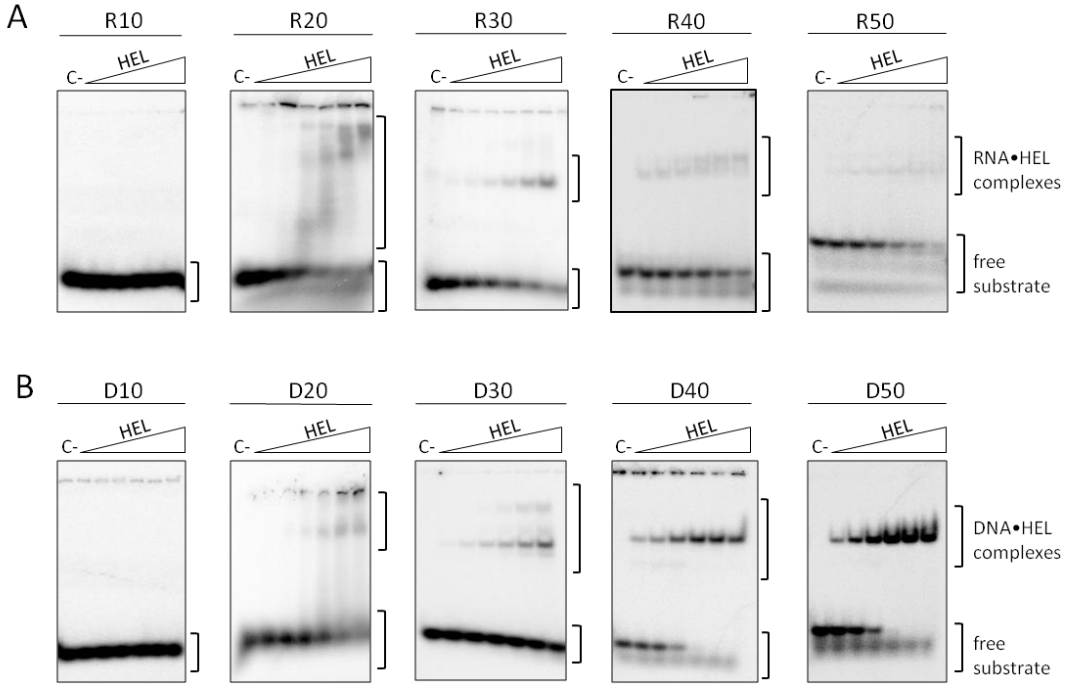

Figure 4. Nucleic acid binding activity of HEL. (A) EMSA with HEL and 5'-^{32}P-labeled single-stranded RNAs (ssRNAs) (2.5 nM): R10, R20, R30, R40, R50. **(B)** EMSA with HEL and 5'-^{32}P-labeled single-stranded DNAs (ssDNAs) (2.5 nM): D10, D20, D30, D40, D50. Increasing amounts of HEL (2.97, 5.94, 11.86, 23.75, 47.5, 95 μM) are represented by a triangle. Reaction mixtures were incubated at room temperature for 15 min. (C-) − a control sample with no protein.

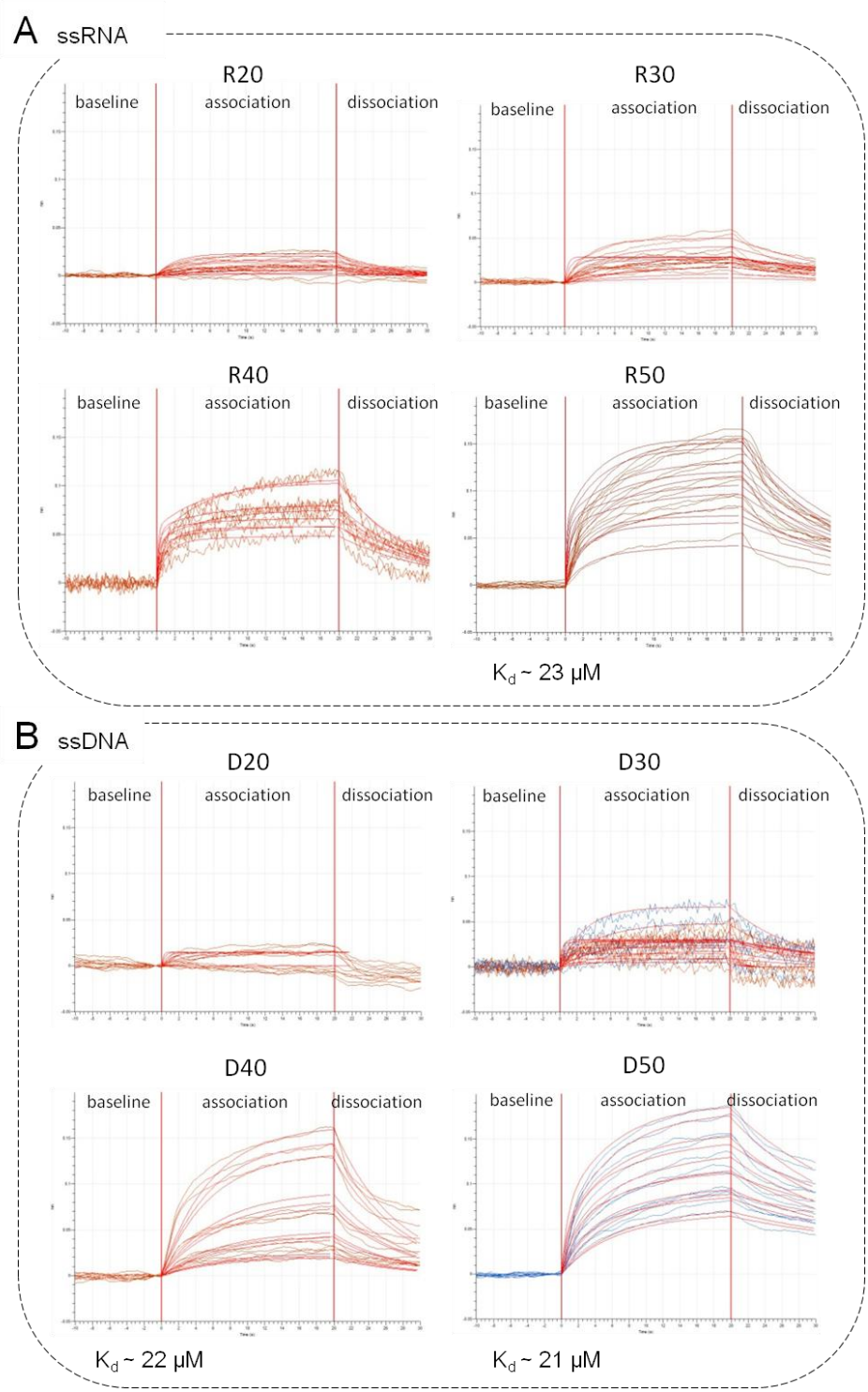

Figure 5. Binding curves obtained using bio-layered interferometry (BLI) method for (A) ssRNAs and (B) ssDNAs and HEL. In the experiment, HEL (1 μM) was incubated with increasing amounts of ssRNA (3.125, 6.25, 12.5, 25, 50 100 μM): R20, R30, R40, R50; or increasing amounts of ssDNA (3.125, 6.25, 12.5, 25, 50 100 μM): D20, D30, D40, D50. Measurements were carried out at 23 °C.

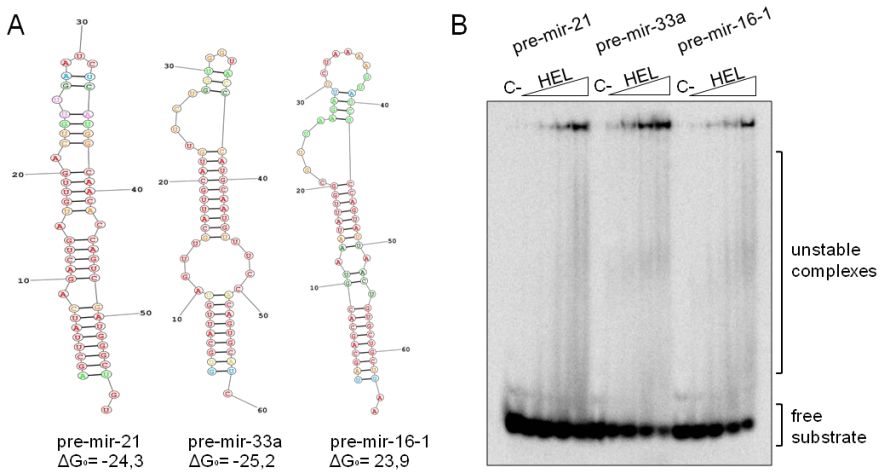

Figure 6. Pre-miRNA binding by HEL. (A) Secondary structures of pre-miRNAs used in the study. The predicted structures for pre-mir-21, pre-mir-33a and pre-mir-16-1, generated by RNAstructure Fold online tool (Mathews Lab) [42], are presented. The structures are color-annotated according to base pairing probability. The free energy values expressed in kcal/mol are shown at the bottom. Nucleotides are numbered starting from the 5'-end. **(B)** EMSA with HEL and 5'-^{32}P-labeled pre-miRNAs (2.5 nM): pre-mir-21, pre-mir-33a, pre-mir-16-1. Increasing amounts of HEL (11.86, 23.75, 47.5, 95 μM) are represented by a triangle. Reaction mixtures were incubated at room temperature for 15 min. (C-) − a control sample with no protein.

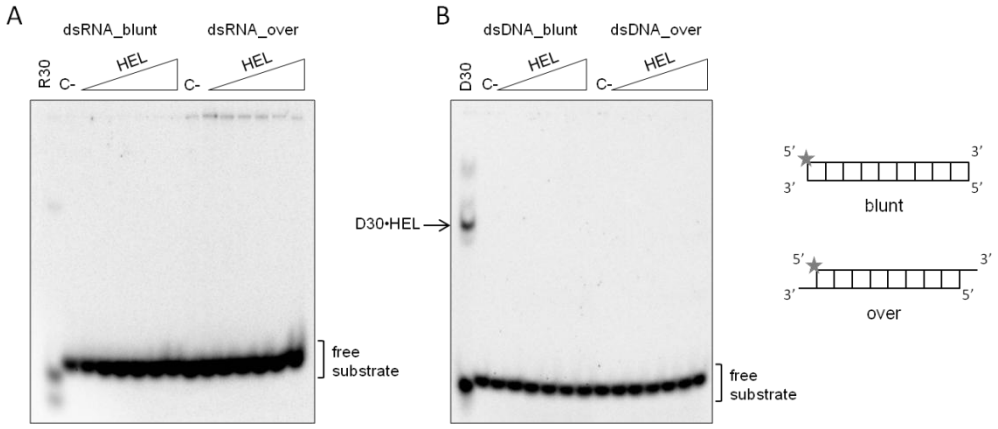

Figure 7. Double-stranded RNA (dsRNA) and double-stranded DNA (dsDNA) binding by HEL. (A) EMSA with HEL and ^{32}P-labeled 32-bp RNA (dsRNA_blunt) (2.5 nM) and 30-bp RNA duplex with a 2-nt 3' overhang on each end (dsRNA_over) (2.5 nM), (R30) – a control sample: ^{32}P-labeled R30 incubated with 95 μM HEL. **(B)** EMSA with HEL and ^{32}P-labeled 32-bp DNA (dsDNA_blunt) (2.5 nM) and 30-bp DNA duplex with a 2-nt 3' overhang on each end (dsRNA_over) (2.5 nM), (D30) – a control sample: ^{32}P-labeled D30 incubated with 95 μM HEL. Increasing amounts of HEL (2.97, 5.94, 11.86, 23.75, 47.5, 95 μM) are represented by a triangle. Reaction mixtures were incubated at room temperature for 15 min. (C-) − a control sample with no protein.

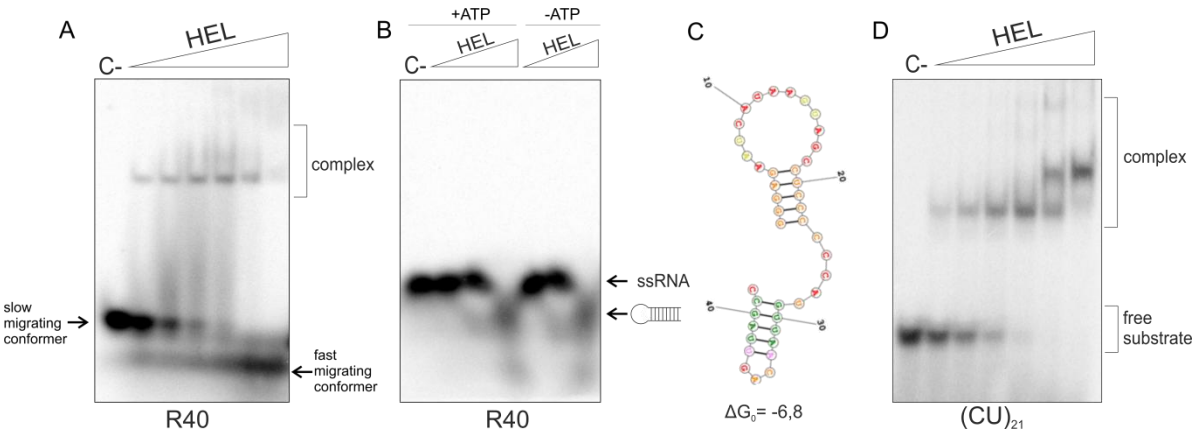

Figure 8. Interactions between 42-nt RNAs and HEL. (A) EMSA with HEL and 5'-^{32}P-labeled R40 (42-nt) (2.5 nM). Increasing amounts of HEL (2.97, 5.94, 11.86, 23.75, 47.5, 95 μM) are represented by a triangle. Reaction mixtures were incubated at room temperature for 15 min. (C-) − a control sample with no protein. **(B)** Native PAGE analysis of the mixtures of 5'-^{32}P-labeled R40 (2.5 nM) and increasing amounts of HEL (5.94, 23.75, 95 μM), represented by a triangle. After 15 min incubation at room temperature, sodium dodecyl sulfate (SDS) to final concentration of 1% was added (SDS is a protein denaturing agent). (C-) − a control sample with no protein. (+ATP) – reaction mixtures with 1 mM ATP. (-ATP) – reaction mixtures without ATP. **(C)** Secondary structure of R40 generated by RNAstructure Fold online tool (Mathews Lab) [42]. The structure is color-annotated according to base pairing probability. The free energy value expressed in kcal/mol is shown at the bottom. Nucleotides are numbered starting from the 5'-end. **(D)** EMSA with HEL and 5'-^{32}P-labeled $(CU)_{21}$ (42-nt) (2.5 nM). Increasing amounts of HEL (2.97, 5.94, 11.86, 23.75, 47.5, 95 μM) are represented by a triangle. Reaction mixtures were incubated at room temperature for 15 min. (C-) − a control sample with no protein.

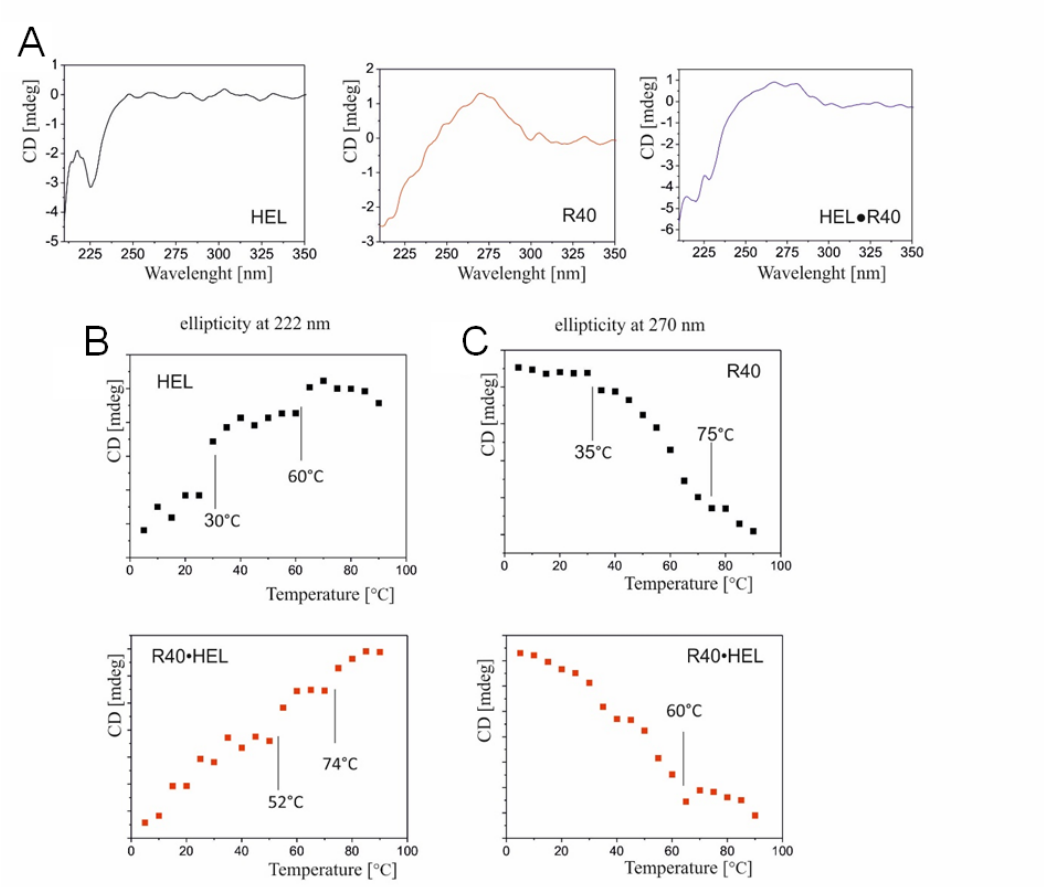

Figure 9. Circular dichroism spectroscopy (CD) analysis of R40, HEL and the HEL•R40 complex. (A) Exemplary CD spectra for: HEL (black), R40 (red), and the HEL•R40 complex (blue). Measurements were carried out at 15 °C. **(B)** CD thermal analysis at 222 nm for HEL (black) and the HEL•R40 complex (red). **(C)** CD thermal analysis at 270 nm for R40 (black) and the HEL•R40 complex (red).

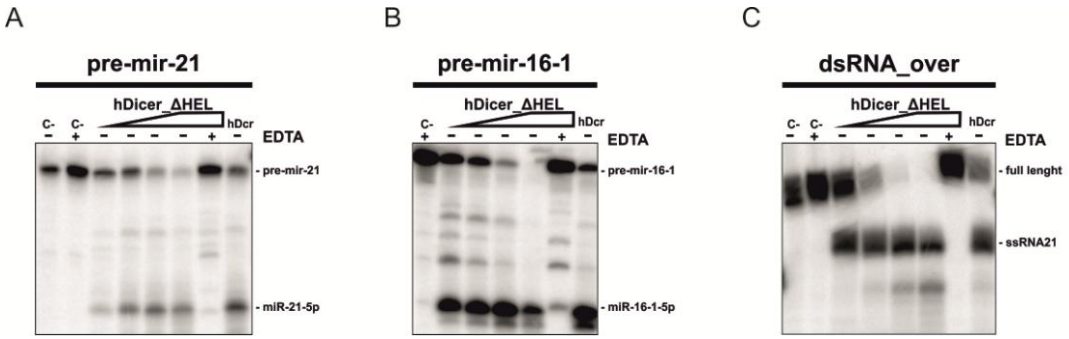

Figure 10. RNase activity assay of hDicer_ΔHEL. (A-C) The results of the *in vitro* assays involving: **(A)** pre-mir-21 (5 nM), **(B)** pre-mir-16-1 (5 nM), **(C)** 30-bp dsRNA_over with 2-nt 3'-overhangs (5 nM), and increasing amounts of hDicer_ΔHEL (1.25; 2.5; 5; 10 nM), represented by a triangle. Reaction mixtures were incubated at 37 °C for 30 min. (C-) controls containing only the substrate in the reaction buffer. (C+) controls contained the substrate in the reaction buffer with the addition of the Mg^{2+}-chelating agent, EDTA (25 mM). (+EDTA) supplementation of the reaction buffer with 25 mM EDTA. As a positive control, the WT hDicer (hDcr) preparation was used (10 nM).

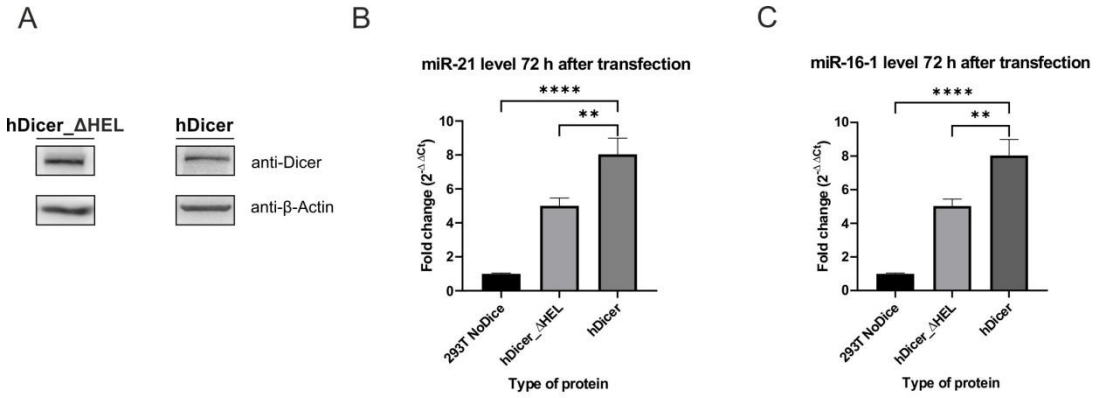

Figure 11. Comparison of miRNA levels produced in NoDice cells expressing hDicer_ΔHEL and WT hDicer. (A) Western blot analysis of hDicer_ΔHEL and the wild-type hDicer (hDcr) expressed in 293T NoDice cells. Cells were harvested and analyzed by Western blotting with anti-hDcier and anti-β-actin antibodies 72 h after transfection with the respective expression plasmids. **(B, C)** Results of the RT-qPCR analysis of the level of the endogenous mature: **(B)** mir-21-5p and **(C)** mir-16-1-5p, in the 293T NoDice cells (a negative control), or 293T NoDice cells expressing either hDicer_ΔHEL or hDcr. 72 h after transfection, cells were harvested and total RNA was isolated. miRNA levels were determined by RT-qPCR and normalized to the expression of U6 snRNA, as a reference gene. The values are averaged from three biological replicates as mean SD. Data were analyzed by a one-way ANOVA test followed by Dunnett's multiple comparisons tests. The obtained p values are as follows, for miR-16-1: ** $p < 0.0021$, **** $p < 0.0001$; for miR-21: ** $p < 0.0040$, **** $p < 0.0001$.